Uncertainty budgets for liquid waveguide capillary cell (LWCC) CDOM absorption measurements

INA LEFERING,[1*] RÜDIGER RÖTTGERS,[2] CHRISTIAN UTSCHIG,[2] DAVID MCKEE[1]

[1]*Physics Department, University of Strathclyde, Glasgow, Scotland, UK*
[2]*Remote Sensing Department, Helmholtz-Zentrum Geesthacht, Geesthacht, Germany*
**Corresponding author: katharina.lefering@strath.ac.uk*

Received XX Month XXXX; revised XX Month, XXXX; accepted XX Month XXXX; posted XX Month XXXX (Doc. ID XXXXX); published XX Month XXXX

Long pathlength liquid waveguide capillary cell (LWCC) systems using simple spectrometers to determine the spectral absorption by coloured dissolved organic matter (CDOM) have previously been shown to have better measurement sensitivity compared to high-end spectrophotometers using 10 cm cuvettes. Information on the magnitude of measurement uncertainties for LWCC systems, however, has remained scarce. Cross-comparison of three different LWCC systems with three different pathlengths (50 cm, 100 cm, and 250 cm) and two different cladding materials enabled quantification of measurement precision and accuracy, revealing strong wavelength dependency in both parameters. Stable pumping of the sample through the capillary cell was found to improve measurement precision over measurements made with the sample kept stationary. Results from the 50 cm and 100 cm LWCC systems, with higher refractive index cladding, showed systematic artefacts including small but unphysical negative offsets and high frequency spectral perturbations due to limited performance of the salinity correction. In comparison, the newer 250 cm LWCC with lower refractive index cladding returned small positive offsets that may be physically correct. After null-correction of measurements at 700 nm, overall agreement of CDOM absorption data at 440 nm was found to be within 5% RMS%E.

OCIS codes: *(010.1030) Absorption; (010.4450) Oceanic optics.*

http://dx.doi.org/ xxx

1. INTRODUCTION

The spectral absorption of light yields information on the presence and concentration of absorbing constituents within a natural water sample. While water itself absorbs strongly in the near-infrared (NIR) region of the spectrum, non-water constituents typically absorb most strongly at visible and ultra-violet (UV) wavelengths, with only limited signals in the NIR [1]. For example, phytoplankton have a characteristic absorption spectrum which is composed of the absorption by different pigments present in the cells, with typically two absorption peaks in the blue and red spectral region and negligible absorption in the NIR. The absorption of other organic components such as particulate detrital material and coloured dissolved organic matter (CDOM), increases continuously with decreasing wavelength, with maximum absorption in the UV (< 300 nm) [2].

Light absorption by CDOM is well known to play an important role in aquatic environments, contributing to a variety of biogeochemical processes and the light propagation underwater [3-5]. For example, CDOM absorption might protect phytoplankton from damaging UV radiation [6, 7] and, at the same time, limit the amount of light available for photosynthesis and, hence, hinder primary production [8, 9]. Knowledge on CDOM absorption spectra is relevant for the correct interpretation of ocean colour remote sensing signals, such as for the retrieval of chlorophyll a concentrations [10, 11], and the parameterisation of primary production models [7]. The spectral slope can provide additional information on the origin of the material (e.g. marine or terrestrial) which can be used for monitoring of river discharge processes, and on the chemical composition [12]. CDOM absorption is highly variable and typically highest in fresh water systems and rivers, generally decreasing with distance from shore [13]. In the past, a strong link between CDOM concentration and salinity has been demonstrated in coastal waters where conservative mixing of river and oceanic water is likely to influence CDOM absorption [14-16]. CDOM has also been utilised as tracer for changes in biogeochemistry and circulation of water masses [11, 17, 18]. Some recent studies have investigated CDOM absorption and its influence on solar heating of the upper ocean, in particular for Arctic regions [19, 20].

CDOM light absorption coefficients, a_{CDOM}, are determined spectrophotometrically from natural water samples which have been filtered through a 0.2 µm pore size filter. This has traditionally been done using bench-top spectrophotometers equipped with quartz-glass cuvettes and a typical pathlength of 10 cm, e.g. [2]. However, this method is not sensitive enough, particularly in the visible spectral region, to measure absorption by CDOM in oceanic waters where concentrations are extremely low. More recent studies have therefore used measurement systems with longer optical pathlengths such as liquid core waveguide cells [21] or point-source integrating cavity

absorption meters (PSICAM) [22]. The latter are complex, require large sample volumes, have a relatively limited spectral range, and have therefore not been routinely used. Liquid core waveguide systems, however, are compact, fairly simple to operate and have found increased application in aquatic studies.

There are currently two different types of cells used for the determination of absorption by natural water samples: (1) the multiple pathlength UltraPath system manufactured by World Precision Instruments Inc. (WPI), US, [23, 24] and (2) single pathlength liquid waveguide capillary cells (LWCC, also WPI) [21]. In both cell types light is guided through the cell containing the sample using internal reflections at the cell walls. The main difference between the two types is the capillary's optical construction (see [25]). The UltraPath is a Type I cell with large inner diameter, made from a very low refractive index (less than water) polymer (Teflon) allowing total internal reflection of light directly at the water to cell surface. LWCCs are Type II small inner diameter cells, where low refractive index material is used as a cladding around a transparent quartz-glass tubing. This construction reduces contamination issues and minimises problems due to adhesion of air bubbles [26]. Light penetrating the quartz-glass tubing before being reflected on the outer Teflon cladding leads to a visible high frequency pattern (when using spectrometers with high optical resolution) which changes with the refractive index of water, i.e. with salinity. The exact mechanism for this high frequency pattern remains essentially unknown. For both types of cells, the quality of the capillary performance depends on the absolute refractive index of the polymer, i.e., the absolute difference to the refractive index of (sea-)water. Available LWCC pathlengths range from 50 cm to 500 cm while an UltraPath system allows choice from multiple pathlengths between 2 and 200 cm to be used with a single instrument.

Liquid waveguide measurement systems typically consist of a cell, a stable light source and a spectral detector. These systems are compact, without any moving parts and, thus, less susceptible to ship movement than traditional cuvette measurements in spectrophotometers. Waveguide cells only require small sample volumes, 125 µL – 1.25 mL for LWCCs and < 10 mL for UltraPath cells. However, small volumes of samples can heat up very quickly inside the cell, leading to a higher susceptibility to temperature changes that influence light absorption at NIR wavelengths. Heating of the sample can further result in degassing and build-up of gas bubbles. The presence of bubbles inside the cell results in increased scattering and potential overestimation of absorption. In addition, air bubbles inside the cell are a major issue because air has a higher compressibility relative to water and long-pathlength measurements become extremely sensitive to changes in the sample injection pressure, which can be observed as relatively large negative offsets (~ -0.02 m^{-1}). This is a considerable disadvantage compared to other spectrophotometric systems like a cuvette spectrophotometer or a PSICAM where samples do not have to be injected. Given the smaller sample volume required and the lower risk of contamination and adhesion of air bubbles, the LWCC is potentially preferable over an UltraPath cell.

UltraPath systems have found application in seawater studies [17, 18]. LWCC systems have predominantly been used for opto-chemical analysis with non-saline waters and only in very few marine studies, e.g. [27, 28]. A remaining concern is the lack of information on the magnitude of measurement uncertainties and information on the performance of these systems. Some work has been done in the past, predominantly focussing on UltraPath systems [29], and, to our knowledge, no comparable investigation has been carried out for the type II LWCC systems. This work will present an optimized procedure to reduce the influence of scattering by particles and small bubbles on CDOM absorption coefficient determinations and compare absorption measurements from three different pathlength LWCCs (50 cm, 100 cm, and 250 cm). The investigation will include a comparison of the precision and accuracy for different pathlengths and look at the effects of applying pressure versus not applying pressure to the sample during measurement recording.

2. METHODS

A. Sampling

Absorption data were collected during a cruise on *RV Heincke,* circumnavigating Great Britain, in spring 2015. The 62 sample sites included the English Channel, Bristol Channel, several Scottish sea lochs, the East Coast of Scotland close to the River Tay and River Forth estuaries as well as the central North Sea (Fig. 1). A variety of water types was sampled including sediment dominated estuaries, various coastal waters and the onset of the phytoplankton spring bloom in Loch Fyne. Water samples were collected using Niskin bottles mainly at depths close to the surface (top 10 m) but datasets also include a few samples from greater depths, up to 85 m. On board, samples were divided into two sub-samples which were processed independently by two different groups from (1) the Helmholtz-Zentrum Geesthacht ('HZG') and (2) the University of Strathclyde ('Strath'). Both groups used their own filtration systems to prepare CDOM samples by two-step filtration. Both groups used their own filtration systems to prepare CDOM samples by two-step vacuum filtration. First, samples were filtered through a 47 mm GF/F filter (Whatman, Germany) with a typical pore size of 0.5 µm [30] and then through 47 mm Nitrocellulose membrane filters with a 0.22 µm pore size (GSWP, Merck Millipore Ltd., Ireland). After filtration, the samples were stored in a water bath to stabilise at room temperature (same as the purified water reference) and measured within a few hours of collection.

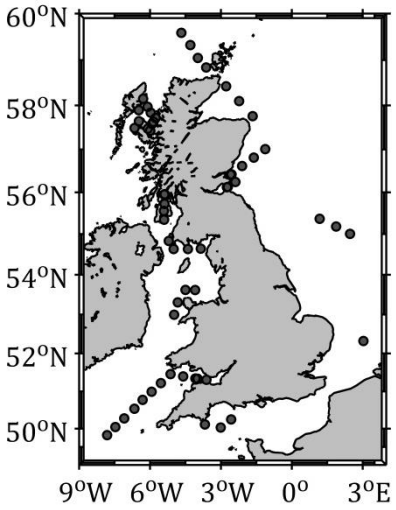

Fig. 1. Sampling sites during a 20-day cruise in April 2015.

B. Absorption determination

CDOM absorption spectra were determined from measurements using Type II liquid waveguide capillary cells (World Precision Instruments Inc., US) connected to Deuterium Halogen UV/VIS light sources (DH-2000-BAL, Ocean Optics Inc., US) and photo-diode array spectrometers (AvaSpec ULS2048XL, Avantes, Netherlands) using optical fibres. Samples were measured by the two groups using two slightly different set-ups. The Strath measurement system used a 100 cm LWCC (LWCC-2100) and a VIS to near-infrared spectrometer; the HZG group used LWCCs of two pathlengths, 50 cm (LWCC-2050) and

250 cm (LWCC-3250), and the UV to VIS version of the spectrometer. The set-up control, measurement recording and data storage were done using a Python routine developed in the HZG group. The absorption by CDOM was determined in triplicate from 300 – 750 nm against purified water (Milli-Q, water purification system: Millipore, Ireland) as reference. Samples were injected into the capillaries through Spartan syringe filters (Whatman, Germany) with a 25 mm diameter and 0.2 µm pore size using clear plastic syringes. HZG syringe filters were cleaned with purified water before use until no absorption difference in the UV (at 250-300 nm) was observed between filtered and unfiltered purified water in the LWCC set-up. Strath syringe filters were cleaned by rinsing with 50 mL of Milli-Q. This additional sample filtration under pressure through syringe filters was found to improve the stability of signals compared to injection of samples filtered under vacuum only. Vacuum filtered samples often showed a rather wavelength independent and sometimes strong positive bias, that is interpreted as scattering by microbubbles that build up during or after the vacuum filtration by degassing due to pressure differences across the filter membrane. These microbubbles were found to be stable for a very long time. The pressure filtration during sample injection into the cell was found to remove microbubbles and, hence, the bias. For consistency purified water for reference measurements was injected into the capillary through the same syringe filter, with continued injection until the signal reached previous reference levels. The HZG protocol recorded spectra while sample was slowly, manually pumped through the cell, keeping the pressure applied to the syringe as steady as possible. The Strath approach used a stationary sample, i.e. with no pressure applied to the system in the moment a measurement was taken. For the latter, three different syringes were used: two for purified water (one for a pre-flush to minimise contamination, one for the reference) and one to inject the sample. Measurements were recorded as quickly as possible to minimise temperature effects as no further temperature correction was applied here. Dark current signals were collected by closing a shutter in the lamp and recording spectra. Sample and reference intensity spectra were collected, corrected for dark currents by subtraction, and used to calculate absorption coefficients using the Beer-Lambert law with nominal pathlengths provided by the manufacturer for each LWCC. Data with optical densities greater than 1.5 were found to be subject to problems associated with detector non-linearity and straylight, and were therefore excluded from further analysis.

C. Salinity correction

The presence of salt ions in seawater introduces a change in absorption relative to pure water that is significant at red/NIR wavelengths [31]. LWCC measurements are further affected by changes in the refractive index caused by variations in the salinity of the sample, resulting in the formation of high frequency structures in recorded spectra when using detectors with high sensitivity and fine spectral resolution (Fig. 2). This high frequency pattern is not typically observed with lower spectral resolution detectors (< 5 nm), and is slightly variable, typically changing with each (dis)assembly of the kit. Salinity correction coefficients are system-specific (combining water and LWCC effects) and were determined by measuring the absorption of a freshly prepared NaCl solution multiple times during the 20-day cruise (5 times for the 50 cm and 100 cm cell and 3 times for the 250 cm cell) following the suggestions in [32]. The NaCl solution was prepared by adding 100 mL of purified water to 10 g of NaCl (> 99.5%; Sigma-Aldrich, Germany), resulting in a concentration of approx. 90.9 g kg^{-1}. This relatively strong, single concentration was used to minimise the effort going into the determination of correction coefficients whilst increasing the signal-to-noise ratio compared to using a concentration closer to the sample salinity. It has been shown in the past that the optical effect of an NaCl solution increases linearly with concentration, e.g. [31]. Therefore, final correction coefficient, as shown in Figure 2, can be derived by dividing the measured NaCl absorption spectra by the concentration. To correct CDOM absorption spectra for salinity effects, correction coefficients were scaled to the corresponding sample salinity (in g kg^{-1}) and subtracted according to Eq. 1.

$$a_{corrected}(\lambda) = a_{measured}(\lambda) - S \times \psi_S(\lambda) \quad \textbf{(1)}$$

where $a_{corrected}$ is the absorption coefficient corrected for salinity effects, $a_{measured}$ is the uncorrected absorption coefficients, S is the sample salinity and Ψ_S is the salinity correction coefficient.

Röttgers et al. [32] showed that salinity correction coefficients determined using either a NaCl solution or artificial seawater are comparable in the visible range. They also found that artificial seawater salts suffer more strongly from contamination issues due to the presence of other salts containing optically impure halogen ions. Contamination cannot easily be removed by combustion and artificial seawater therefore gives less reliable results at wavelengths < 500 nm. Salinity correction coefficients are expected to become increasingly negative into the blue/UV following the trend in absolute differences in refractive indices of pure water and salt solutions. Although measurements were stable over the course of the cruise, at UV/blue wavelengths (< 450 nm) there was increased variability and measured spectra did not follow the expected negative trend but tended to be artificially high which is assumed to be due to impurities of the sodium chloride solution. The effect of salinity on absorption was smallest for the longest pathlength and increased with shorter pathlengths. The salinity of each sample was recorded and CDOM spectra were corrected using the average of all sodium chloride spectra of each LWCC scaled to the salinity of the sample.

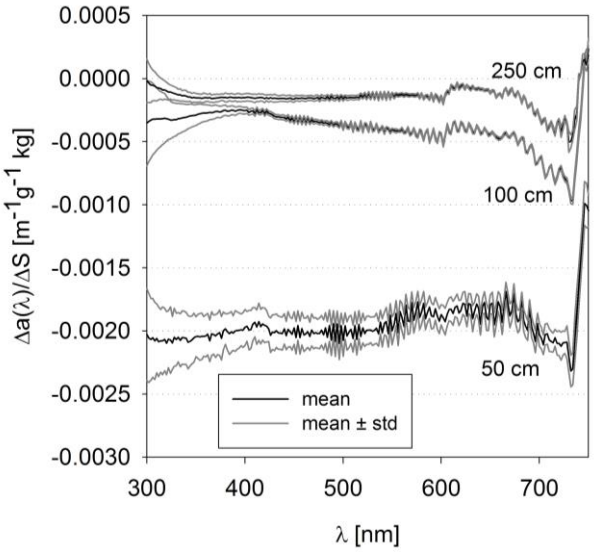

Fig. 2. Mean (black) and corresponding standard deviation (grey) spectra of salinity (where salinity is expressed as salt concentration in g kg^{-1}) correction coefficients derived for the three LWCC systems.

D. Assessment and statistic descriptors

Geometric mean linear regressions were applied to find best-fit slopes and offsets with corresponding 95% confidence intervals in order to assess the performance of the two longer pathlengths in comparison to the 50 cm LWCC cell.

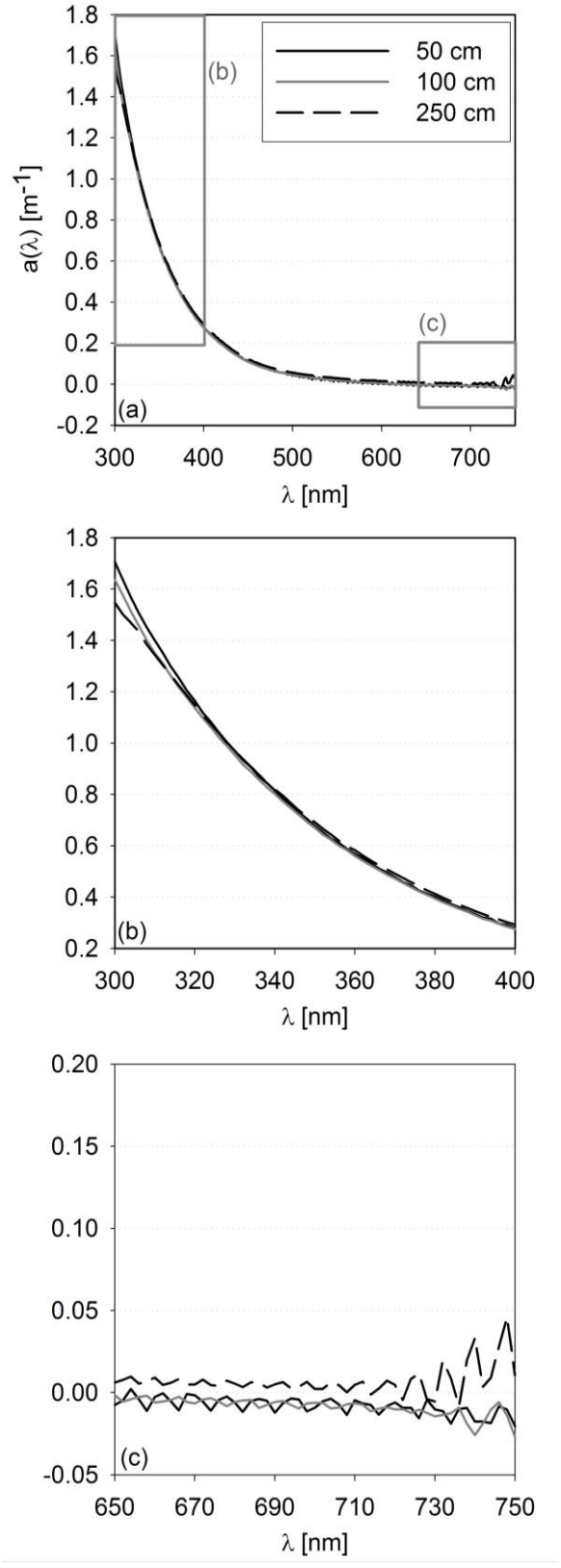

Fig. 3. CDOM absorption spectra measured with 3 LWCC systems with 3 different pathlengths (50 cm, 100 cm, and 250 cm) for selected spectral regions: (a) 300 – 750 nm, (b) 300 – 400 nm, (c) 650 – 750 nm. Note changing scales on y-axes.

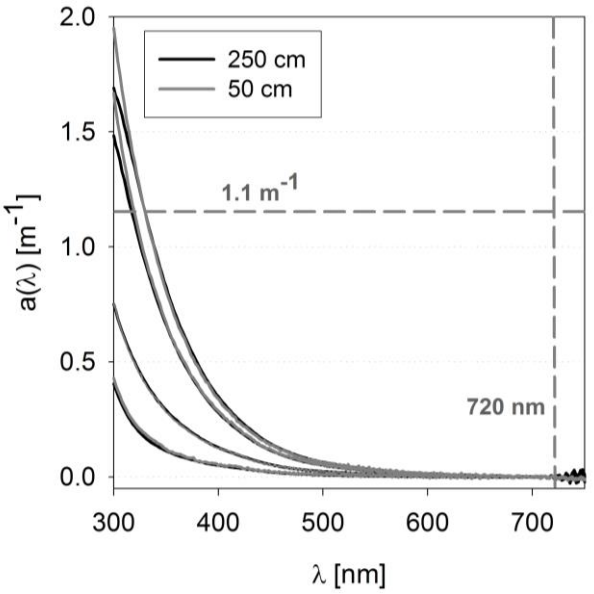

Fig. 4. Absorption spectra for four samples with different CDOM concentrations measured with two different LWCC systems (50 cm and 250 cm). All spectra have been null-corrected at 700 nm. Grey dashed lines highlight where data has been excluded from analysis: for 250 cm pathlength only absorption values < 1.1 m^{-1} were considered to minimise detector related artefacts and all data at wavelengths > 720 nm was excluded to avoid an influence of the temperature effects.

Additionally, root mean square errors, RMSE (Eq. 2), and root mean square percentage errors, RMS%E (Eq. 3), calculated for the whole dataset provided information on the absolute and relative deviation between data determined using the longer capillary cells, a_i, (with i being either 100 cm or 250 cm) and absorption measured with the 50 cm pathlength, $a_{50\,cm}$.

$$RMSE = \sqrt{\frac{1}{n}\sum_{1}^{n}\left(a_i - a_{50cm}\right)^2} \quad \textbf{(2)}$$

$$RMS\%E = \sqrt{\frac{1}{n}\sum_{1}^{n}\left(\frac{a_i - a_{50cm}}{a_{50cm}} \times 100\right)^2} \quad \textbf{(3)}$$

3. RESULTS

A. Absorption spectra

The performance of CDOM absorption determinations with different pathlength LWCC systems was assessed from 300 nm – 750 nm at 2 nm resolution. Fig. 3a shows an example spectrum for a selected station and highlights some of the features observed at the edges of the spectrum. Measurements with the 250 cm pathlength cell show features associated with limited signal-to-noise ratio at both edges of the spectrum. In the NIR, strong water absorption reduces the transmitted signal significantly whereas strong sample absorption in combination with reduced detector sensitivity and low lamp output reduce signals at UV/blue wavelengths towards the signal-to-noise limit. This results in non-linear behaviour which can be observed as systematic curving off and underestimation of the absorption spectra when sample absorption is high (> 1.1 m^{-1}; Fig. 3b & Fig. 4).

In the two shorter pathlengths, 50 cm and 100 cm, signals are not attenuated as strongly and no systematic curve-off was observed in the

wavelength range used for this work, (Fig. 3b). For the following analysis, data measured with the 250 cm capillary were therefore limited to absorption values < 1.1 m^{-1} to avoid artefacts due to sensitivity limitations. Despite the imposition of this restriction, remaining spectra extended at least down to 334 nm.

Absorption spectra measured with the 50 cm and 100 cm LWCCs showed consistently significant negative offsets at red/NIR wavelengths even after the correction for salinity effects (Fig. 3c). Therefore, an offset correction was applied before subsequent analysis using averages calculated from 690 – 710 nm, with overall average offsets of -0.0074 m^{-1} and -0.0103 m^{-1} for the 50 cm and 100 cm pathlengths, respectively. Data obtained using the 250 cm LWCC did not exhibit negative offsets once measurements were corrected for salinity effects. This is presumably due to the fact that the LWCC-3250 capillary cell has a cladding of a material with lower refractive index than the two shorter cells of the LWCC-2000 series (Mathias Belz, WPI, pers. comm.). The lower refractive index of the cladding leads to a higher optical transmission through the capillary and much lower refractive index effects by seawater when compared to purified water. Positive NIR absorption signals from the newer LWCC-3250 capillary cell may represent genuine non-zero CDOM absorption. However, the necessity to offset correct the shorter pathlength data resulted in a methodological inconsistency between datasets that could only be resolved by also offset correcting the 250 cm data.

Furthermore, the absorption in the NIR is strongly affected by the temperature dependency of pure water absorption which occurs when reference and sample temperature differ. These effects were not corrected as they are a result of small sample volumes being rapidly warmed during passage of the sample through the LWCC. There is no practical means to measure the temperature of samples inside the LWCC but the effects, as observed in spectral features around 750 nm, were generally low. The magnitude of the effect was greatest for the longest cell (250 cm) due to strong amplification of temperature induced signal changes along the pathlength. The comparison of the performance of the different set-ups was limited to wavelengths < 720 nm to avoid bias due to temperature artefacts (Fig. 4).

When comparing the performance of the three different capillary cells, it became apparent that the signal-to-noise ratio (observed as fine scale structure in measured spectra) improved with pathlength (Fig. 5). The signal-to-noise was influenced by the sensitivity of the system and the strength of the high frequency pattern caused by the high refractive index of the saline sample which often remains even after applying a salinity correction. Remaining features of this high frequency pattern post-salinity correction presumably originated from differences in the refractive index of a high concentration sodium chloride solution compared to natural seawater and can generally be fully removed during post-processing by smoothing (not applied in this work).

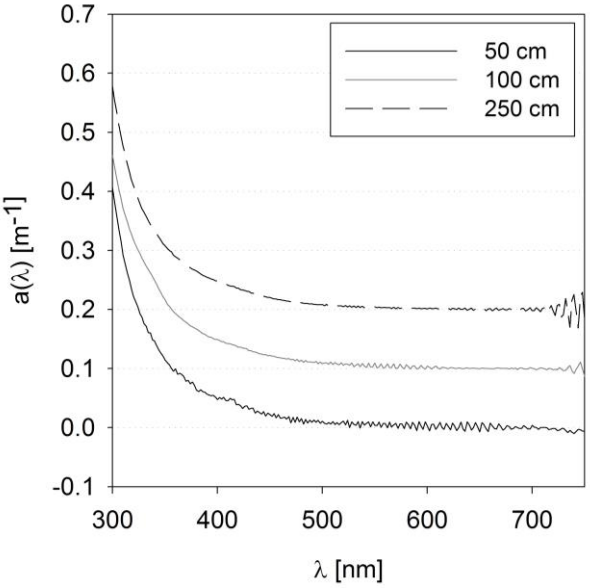

Fig. 5. Comparison of signal-to-noise in measurements with three different pathlength LWCC systems for the same sample (ST 47). Longer pathlength spectra have been offset for clarity by + 0.1 m^{-1} and + 0.2 m^{-1} for the 100 cm and 250 cm pathlength, respectively.

B. Precision

Measurement precision and its dependence on the pathlength of a LWCC were assessed by looking at the standard deviation of triplicate measurements. Figure 6 shows histograms of the standard deviation determined at 440 nm for each of the LWCCs. Measurements with the 100 cm pathlength showed highest standard deviation and widest spread (Fig. 6b).

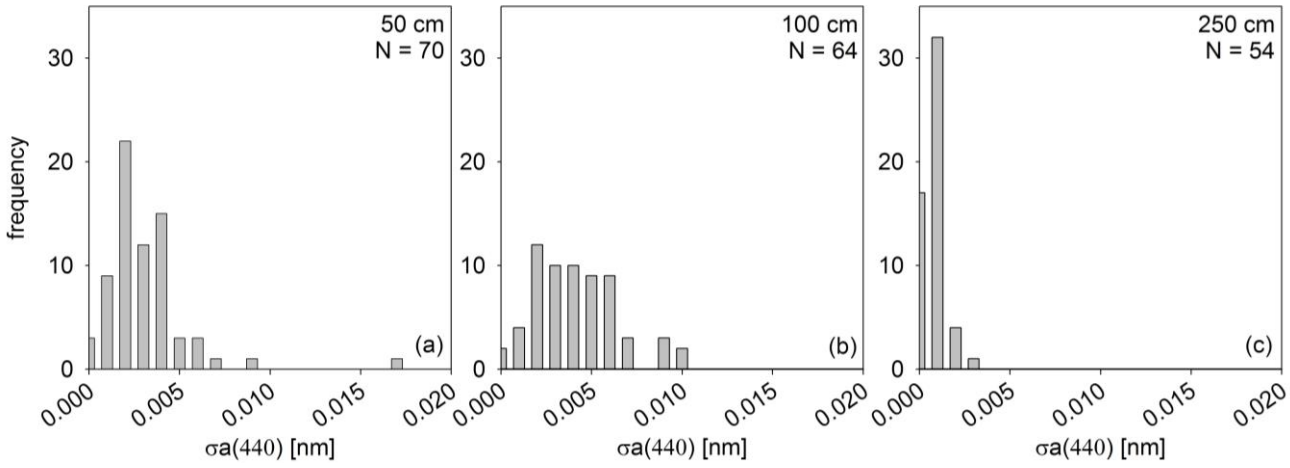

Fig. 6. Measurement precision of three LWCC systems with three different pathlengths: (a) 50 cm, (b) 100 cm, (c) 250 cm. Measurements for (a) and (c) were recorded while sample was pumped through the cell, data shown in (b) war recorded under stationary conditions. Histograms show standard deviations derived from triplicates of absorption measured at 440 nm.

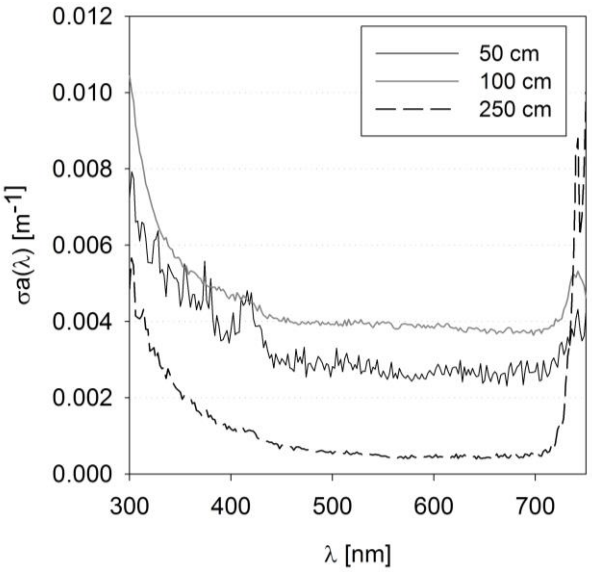

Fig. 7. Average spectral standard deviation of all samples collected, measured with three different pathlengths. Measurements with the 50 cm and 250 cm pathlength were performed while the sample was in-flow whereas measurements in the 100 cm capillary cell were recorded when no pressure was applied to the syringe.

Absorption data measured with the 50 cm cell exhibited overall lower standard deviation compared to the 100 cm LWCC (Fig. 6a) despite the shorter pathlength limiting its sensitivity. This was presumably due to the advantages of in-flow measurements compared to stationary flow conditions. The standard deviation determined for the 250 cm cell showed lowest spread in the data and overall highest precision (Fig. 6c). The comparison of measurements made with the 50 cm and 250 cm LWCCs, using the same approach of continuous manual sample pumping demonstrates how the increase in pathlength improves sensitivity, precision and repeatability of LWCC absorption measurements.

The average spectral standard deviation showed the same pattern (Fig. 7) with regards to precision level, with lowest precision for measurements made in the non-pressurised 100 cm cell. Lowest standard deviations were achieved using the 250 cm LWCC, except at wavelengths greater 720 nm where elevated standard deviations were observed. Results also show that the precision is wavelength dependent, relatively flat from 450 – 700 nm but strongly increasing towards both edges of the spectrum where light intensity levels drop towards the detection limit. No correlation between magnitude of the standard deviation and the absorption signal could be observed (data not shown). Measurements made with the 250 cm LWCC showed most rapid decline of the precision at wavelengths > 720 nm caused by high sensitivity to temperature changes which is enhanced by the long pathlength. This confirms the necessity to constrain the comparison of NIR data to wavelengths < 720 nm. In the blue/UV spectral region, average standard deviations increase exponentially for all three LWCCs. However, this systematic reduction in measurement precision is relatively small compared to the sample absorption at these wavelengths.

C. Accuracy – instrument comparison

Absorption data measured with the three different LWCCs were compared against each other to assess the consistency of the method. Results can provide a first indication of the accuracy of LWCC absorption coefficient measurements. Figure 8 and Figure 9 show data obtained with the 2 longer pathlengths plotted against data measured with the 50 cm pathlength LWCC, following a linear relationship with an R^2 of 0.9970 for the 100 cm and 0.9983 for the 250 cm pathlength (Table 1). Slopes derived from geometric mean linear regressions applied to the data were close to unity, 0.981 ± 0.001 (100 cm) and 1.007 ± 0.001 (250 cm). Regression offsets were insignificant, i.e. below the typically observed detection limit. Data were centred around the 1:1-line for both comparisons. Absorption data measured with the 100 cm cell showed slightly wider spread with overall RMS%E of 14% compared to 11% for the comparison 250 cm vs. 50 cm (Table 1). Data spread (i.e. deviation between measurements) increased towards the edges of the spectrum as deviation from 1:1-line. (Figs. 8 and 9).

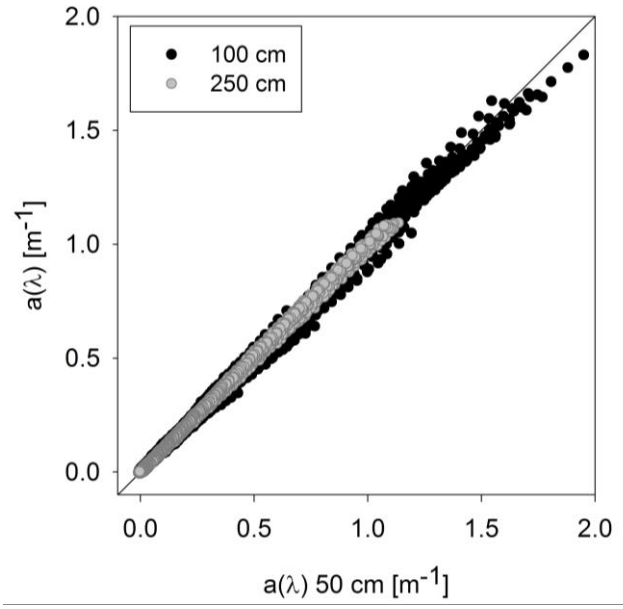

Fig. 8. Comparison of absorption data measured with the 100 cm and 250 cm LWCC against measurements with the 50 cm pathlength, from 300 – 720 nm. Data measured with the 250 cm LWCC system were limited to absorption < 1.1 m^{-1} to avoid non-linearity artefacts at UV wavelengths.

Table 1. Statistical descriptors, slope, offset, R^2 (all obtained from geometric mean linear regression), RMSE, and RMS%E, of absorption spectra measured with the 100 cm LWCC and 250 cm LWCC against measurements with the 50 cm LWCC.

	100 cm LWCC	250 cm LWCC
no of samples	59	44
wavelength range	300 – 720 nm	variable – 720 nm
slope [nm^{-1} m^{-1}]	0.981 ± 0.001	1.007 ± 0.001
offset [m^{-1}]	-0.0005 ± 0.0003	-0.0009 ± 0.0002
R^2 [-]	0.9970	0.9983
RMSE [m^{-1}]	0.0044	0.0040
RMS%E [%]	13.7 %	11.2 %

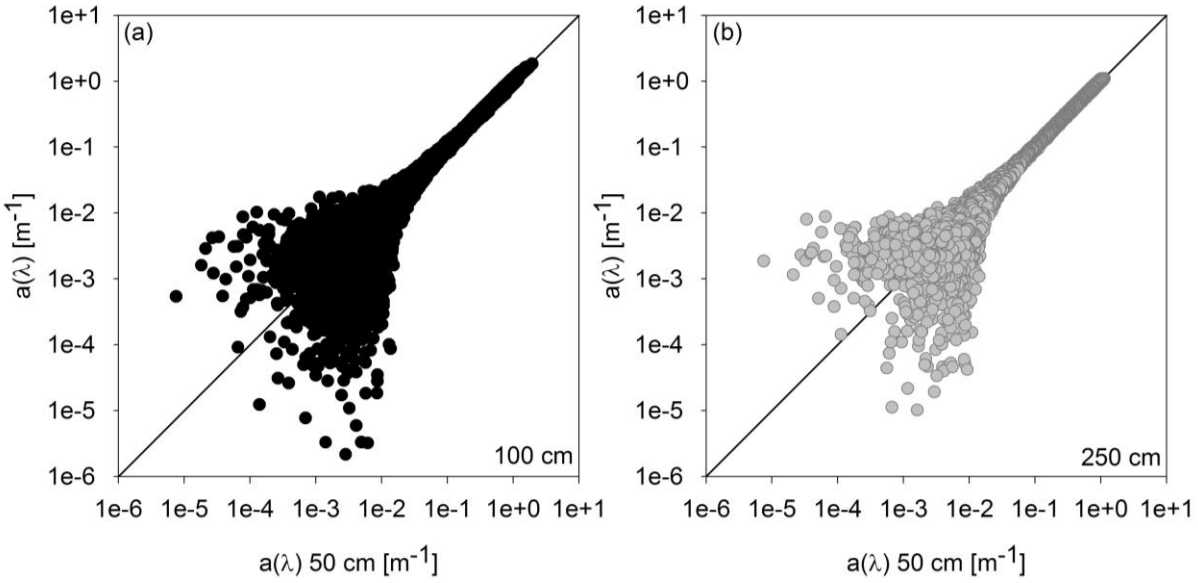

Fig. 9. Comparison of absorption measured with a (a) 100 cm and (b) 250 cm LWCC system against the 50 cm LWCC for wavelengths 300 – 720 nm on a log-log scale. Data measured with the 250 cm LWCC system were limited to absorption < 1.1 m^{-1} to avoid detector related artefacts at UV wavelengths.

D. Spectral analysis of deviation

For a better understanding of the nature of the deviation and its wavelengths dependence, the RMSE and RMS%E were determined spectrally (Fig. 10). Both mean absolute (RMSE) and mean relative (RMS%E) deviations were found to be strongly wavelength dependent. RMS%E values ranged from a few percent in the UV to > 100% at NIR wavelengths (Fig. 10b). The RMSE derived for both the 100 cm and 250 cm LWCCs varied over 1 order of magnitude across the spectrum, with smallest values of 0.001 m^{-1} at NIR wavelengths. Both 100 cm and 250 cm pathlengths showed comparable agreement with the 50 cm cell with RMSE at 440 nm of about 0.004 m^{-1} and RMS%E < 5%, with the 250 cm LWCC showing closer agreement than the 100 cm for wavelengths <350 nm. Figure 10 demonstrates that the overall error is wavelength dependent and shows some variation between different LWCC systems. Unfortunately it is not possible to provide a single, simple statistic to describe the error of this type of measurement as there are a number of features contributing to the overall error (some possibly unknown) and do so in combinations of both absolute and fractional terms. As a result, the error in any individual measurement will vary depending on the optical set-up, the strength of the absorption signal and other factors such as the temperature and salinity of the sample. However, the data presented in Figure 10 may be considered as a rough indicator of the magnitude of errors that might be anticipated for a dataset collected in coastal waters with a_{CDOM}(440 nm) values ranging between 0.011 m^{-1} and 0.157 m^{-1}.

4. DISCUSSION

The determination of CDOM absorption coefficient spectra using LWCCs and a rather simple set-up have been shown to provide a similar accuracy compared to spectrophotometric measurements in a 10 cm cuvette as methodological restrictions (detector issues, lower light source stability, etc.) are compensated by the ability to use much longer optical pathlengths [21]. With the longest pathlength, they allow a higher sensitivity when absorption coefficients are very low [4]. Although the liquid waveguide technique has increasingly been used for bio-optical studies of the aquatic environment (especially the UltraPath system [17, 21, 25, 33]) information on measurement uncertainties is scarce. During a NASA round robin experiment, CDOM absorption spectra measured with different instruments (including various UltraPath systems and an LWCC system) also showed variable offsets between instruments which were attributed to salinity effects, scattering by small bubbles and contamination [29]. In this work, cross-comparison of three type II LWCC with three different pathlengths, 50 cm, 100 cm, and 250 cm, was used to assess the consistency in the method and investigate measurement uncertainties and their potential sources. Detector and light source influences on the overall performance were reduced by using the same type of instrumentation for all three LWCC set-ups.

In a first step, the average standard deviation derived from triplicates was determined to quantify the precision of each individual set-up. The precision was found to be wavelength dependent and strongly increasing towards the edges of the spectrum. This reflects the underlying wavelength dependency of (1) the lamp output which is low at UV and blue wavelengths and (2) sample absorption which is particularly high in the UV/blue due to the absorption by CDOM and in the NIR due to strong absorption by water itself. Given the preponderance of a_{CDOM}(440 nm) values in the literature, it probably makes sense to provide 440 nm statistics as representative values, but this work emphasises that the true uncertainty requires a more robust expression that is likely to be wavelength dependent.

At NIR wavelengths, the sensitivity of water absorption to changes in sample temperature has an additional adverse effect on the measurement precision in this spectral region. The effect is most dominant in spectra measured with the 250 cm LWCC, presumably because it takes longer for a sample to pass through the longer cell allowing it to heat up more strongly. Monitoring or control of the sample temperature inside the cell is not feasible. Temperature effects, however, are fairly constant and can be corrected manually during post-processing, using absorption coefficients for the temperature dependence of water absorption, e.g. [31, 32], in an iterative approach to establish minimal residual spectral structure in the NIR.

Even after correcting measurements for salinity dependency, two systematic artefacts were observed in the spectra which were

associated with increased refractive index of saline samples: (1) a high frequency oscillation pattern and (2) negative offsets observed for the 50 cm and 100 cm LWCC. Using the same high spectral resolution detector, high frequency patterns are not observed in measurements of freshwater absorption (not shown) but always occurred for the samples measured for this work (salinities > 32 psu). If necessary, spectra can be smoothed using a moving average to minimise this oscillation feature. No smoothing was done for the analysis in this work in order to minimise bias in the comparison due to data processing.

The observed negative offsets for the two shorter pathlength cells are relatively small, compared to typical offsets caused by light scattering due to the presence of (micro-)bubbles inside the cells when using vacuum filtered samples rather than pressure filtered [29]. These small negative offsets were only detectable after optimising the measurement procedure, including significant reduction of scattering effects and improvement of measurement stability (by filtering the sample directly into the LWCC). Insufficient correction of salinity effects could be explained by limitations in the derivation of correction coefficients from a measurement of a weakly absorbing sodium chloride solution, especially with the shorter pathlengths. Another potential source of error is the use of sodium chloride solutions instead of artificial seawater [32] which might not be a sufficient representative of seawater absorption and refractive index. An offset correction was applied to the data forcing spectra through zero at 700 nm. This correction is based on the assumption that the error originating from insufficient salinity correction is constant with wavelength which potentially introduces a systematic error of unknown magnitude to the data. The assumption of zero NIR absorption for null-corrections might not hold in all waters. PSICAM measurements that are not susceptible to scattering errors have shown that CDOM absorption at wavelengths >700 nm can be non-negligible but is usually very low [22]. Therefore, if available, LWCC spectra can also be corrected to match PSICAM data at 700 nm. For the cross-comparison attempted in this study, the magnitude of a flat offset correction is consistent and provides a more meaningful result than would be the case otherwise. Mutual self-correction does not alter the results presented here.

Despite remaining issues regarding the correction of salinity effects, comparison of CDOM absorption data (350 – 750 nm) obtained with the 100 cm cell with corresponding PSICAM data showed an RMSE of 0.0078 m^{-1} at 440 nm and an overall RMS%E of ~15% (data not shown). A total of 58 CDOM absorption spectra were available from both instruments, covering a range of absorption at 440 nm from 0.011 m^{-1} to 0.157 m^{-1}. This level of consistency between two independent datasets is a very encouraging endorsement of the performance of the LWCC approach.

The 50 cm and 250 cm LWCC were part of the same set-up using identical light source, detector, and flow conditions during measurements. The comparison of measurements made with these two capillaries allows an assessment of the effects of different pathlengths on the measurement. Due to the five times longer pathlength and the higher transmission of the new LWCC-3000 series cell, the spectra measured with the 250 cm LWCC are less noisy. However, the combination of low lamp output, sensor sensitivity, and high CDOM absorption results in very low light levels close to the detection limit being transmitted through the cell in the UV/blue. This effect can be observed as underestimation of absorption in the longer pathlength cell. Due to these limitations in the optical set-up, the LWCC pathlength used has to be carefully adapted to the wavelength range of interest and the level of the absorption coefficient of the sample.

The comparison of 50 cm and the 100 cm LWCC set-ups provides information on the combined effects of different detectors, different flow conditions and the overall consistency of the method. As increasing the pressure on the sample inside the cell can result in relatively large negative offsets in measured absorption, it is extremely important to record all sample and reference spectra under the same pressure conditions. Continuously pressurising the system, i.e. recording measurements of sample in-flow, was found to increase measurement repeatability significantly and continuous pumping is highly recommended for high-precision absorption determinations. Integrating a peristaltic pump in the set-up to inject sample with a constant pressure is likely to further improve the measurement stability. Future work is required to assess the benefits of automated sample pumping on the precision of LWCC based determinations of the absorption coefficient of CDOM.

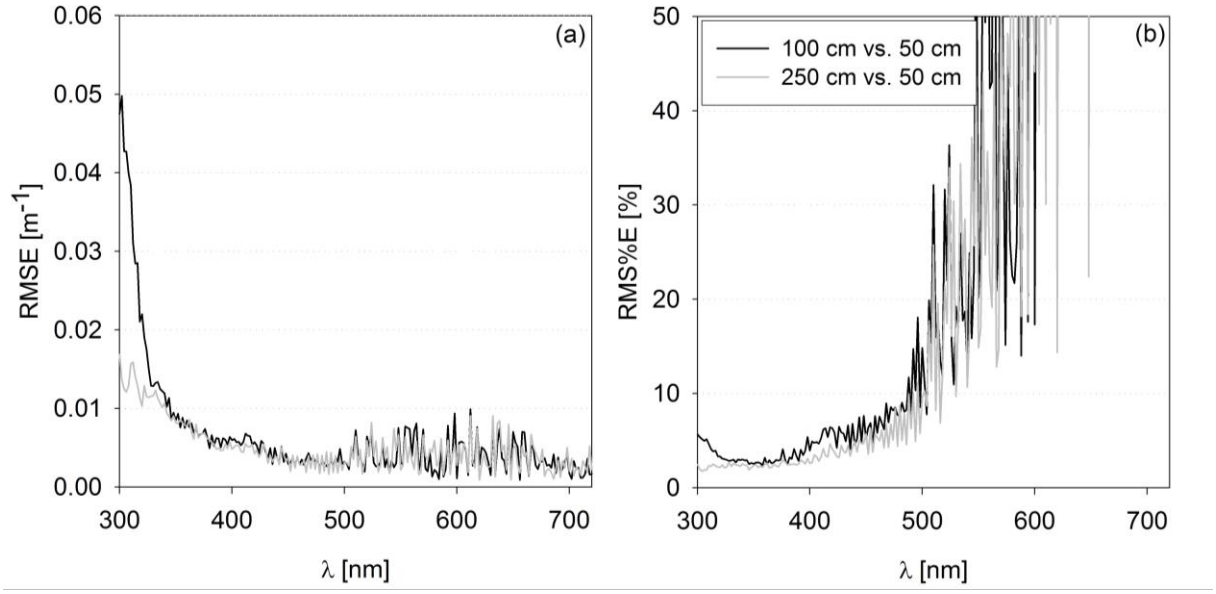

Fig. 10. Wavelength dependency of (a) RMSE (Eq. 1) and (b) RMS%E (Eq. 2) derived from comparison of absorption measured with the 100 cm LWCC and 250 cm LWCC against the 50 cm LWCC.

When the light intensity is generally low, the detector's internal straylight and non-linearity can cause artefacts and lead to a strong underestimation of the absorption coefficient. Analysis of raw intensity spectra showed that the Avantes UV/VIS sensor (used for the 50 cm and 250 cm system) measured a signal of 20 – 50 counts at wavelengths outside the lamp's emission spectrum, i.e. < 180 nm (data not shown). This signal is presumably caused by straylight inside the spectrometer. Tests of a simple straylight correction approach, subtracting the detected signal at 180 nm as a flat offset across the spectrum showed a rather good compensation of the underestimation in measurements with the 250 cm cell. Application of the same correction to data measured with the 50 cm cell showed a smaller effect due to generally higher intensity signals in the shorter cell. The effect of a (constant) straylight correction depends on the pathlength, intensity level, and CDOM concentration and further work is required to develop a suitably robust straylight correction, for example following the suggestion presented in [34] and [35]. The impact of a simple, constant offset straylight correction was fairly small in the visible spectrum. A revised comparison after straylight correction (both 50 cm and 250 cm LWCC) including all data from 300 – 720 nm showed comparable agreement (Table 1), with an RMS%E of 10.5%, RMSE of 0.0042 m^{-1} and a slight trend for the 250 cm to overestimate 50 cm LWCC absorption: 1.021 ± 0.001 (slope), -0.00148 ± 0.0002 (offset), with an R^2 of 0.999. The VIS/NIR detector used with the 100 cm LWCC system did not have any pixels that could be considered outside the lamp's emission spectrum and, hence, no straylight correction was attempted for this set-up.

The assessment of measurement performance of waveguide systems presented here does not cover a comparison of the different cell types, LWCC vs. UltraPath. Previously published studies developing and analysing the UltraPath methodology [18, 33, 36] suggest that determination of CDOM spectra with UltraPath systems can be expected to show a comparable level of performance with advantages and disadvantages discussed above.

5. CONCLUSIONS

The comparison of three different LWCC with three different pathlengths enabled the assessment of measurement uncertainties and data consistency. Results showed good agreement of determined spectral CDOM absorption coefficient data with RMS%E within 5% at 440 nm. The cross-comparison also revealed that it is difficult to come up with meaningful single value statistics to describe the performance of these measurements. Precision and accuracy are both wavelength dependent, reflecting underlying wavelength dependencies in lamp output, sensor sensitivity, internal detector straylight and CDOM absorption characteristics. At the same time, they depend on the pathlength used. Salinity correction for absorption measurements inside a LWCC, derived from a single high concentrated sodium chloride solution appeared to have some limitations and further work is required to minimise remaining systematic measurement errors. Not pressurising the sample inside the cells introduces additional uncertainty to observations compared to constant pressurisation, i.e. in-flow conditions. Artefacts associated with temperature dependence of seawater absorption are significant beyond 720 nm and are not easily controlled or corrected directly but can be addressed in post-processing to some extent. Finally, the requirement for null-correction in the NIR is probably a real limitation that is currently only directly addressed by making alternative measurements, e.g. PSICAM. This, however, is only important for applications where CDOM absorption rather than total absorption (absorption by water itself is dominating) needs to be known with high accuracy at these wavelengths.

Acknowledgment. We thank the captain and crew of FS Heincke for their help and support in data collection. The cruise with RV Heincke was conducted under the grant number AWI-HE442.

REFERENCES

1. B. Wozniak, and J. Dera, *Light absorption in Sea Water* (Springer, 2007).
2. A. Bricaud, A. Morel, and L. Prieur, "Absorption by dissolved organic matter of the sea (yellow substance) in the UV and visible domains," Limnol. Oceanogr. **26**, 43-53 (1981).
3. N. V. Blough, and R. Del Vecchio, "Chromophoric DOM in the coastal environment," in *Biogeochemistry of Marine Dissolved Organic Matter*, D. A. Hansell, and C. A. Carlson, eds. (Academic Press, 2002), pp. *509-546*.
4. N. B. Nelson, and D. A. Siegel, "Chromophoric DOM in the ocean," in *Biogeochemistry of Marine Dissolved Organic Matter*, D. A. Hansel, and C. A. Carlson, eds. (Academic Press, 2002), pp. 547–578.
5. P. G. Coble, "Marine optical biogeochemistry: The chemistry of ocean color," Chemical Reviews **107**, 402-418 (2007).
6. S. A. Green, and N. V. Blough, "Optical-absorption and fluorescence properties of chromophoric dissolved organic-matter in natural-waters," Limnol. Oceanogr. **39**, 1903-1916 (1994).
7. K. R. Arrigo, and C. W. Brown, "Impact of chromophoric dissolved organic matter on UV inhibition of primary productivity in the sea," Marine Ecology Progress Series **140**, 207-216 (1996).
8. K. L. Carder, R. G. Steward, G. R. Harvey, and P. B. Ortner, "Marine humic and fulvic acids - their effect on remote-sensing of ocean chlorophyll," Limnol. Oceanogr. **34**, 68-81 (1989).
9. D. McKee, A. Cunningham, and K. J. Jones, "Optical and hydrographic consequences of freshwater run-off during spring phytoplankton growth in a Scottish fjord," J. Plankton Res. **24**, 1163-1171 (2002).
10. K. L. Carder, S. K. Hawes, K. A. Baker, R. C. Smith, R. G. Steward, and B. G. Mitchell, "Reflectance model for quantifying chlorophyll-a in the presence of productivity degradation products," J. Geophy. Res.-Oceans **96**, 20599-20611 (1991).
11. N. B. Nelson, and D. A. Siegel, "The Global Distribution and Dynamics of Chromophoric Dissolved Organic Matter," Annu. Rev. Mar. Sci. **5**, 447-476 (2013).
12. J. R. Helms, A. Stubbins, J. D. Ritchie, E. C. Minor, D. J. Kieber, and K. Mopper, "Absorption spectral slopes and slope ratios as indicators of molecular weight, source, and photobleaching of chromophoric dissolved organic matter," Limnol. Oceanogr. **53**, 955-969 (2008).
13. E. J. D'Sa, and R. L. Miller, "Bio-optical properties in waters influenced by the Mississippi River during low flow conditions," Remote Sens. Environ. **84**, 538-549 (2003).
14. E. C. Monahan, and M. J. Pybus, "Color, ultraviolet absorbance and salinity of surface waters off west-coast of Ireland," Nature **274**, 782-784 (1978).
15. D. G. Bowers, G. E. L. Harker, P. S. D. Smith, and P. Tett, "Optical properties of a region of freshwater influence (The Clyde Sea)," Estuar. Coast. Shelf Sci. **50**, 717-726 (2000).
16. F. Bengil, D. McKee, S. T. Besiktepe, V. S. Calzado, and C. Trees, "A bio-optical model for integration into ecosystem models for the Ligurian Sea," Prog. Oceanogr. **149**, 1-15 (2016).
17. N. B. Nelson, D. A. Siegel, C. A. Carlson, and C. M. Swan, "Tracing global biogeochemical cycles and meridional overturning circulation using chromophoric dissolved organic matter," Geophys. Res. Lett. **37** (2010).
18. C. M. Swan, D. A. Siegel, N. B. Nelson, C. A. Carlson, and E. Nasir, "Biogeochemical and hydrographic controls on chromophoric dissolved organic matter distribution in the Pacific Ocean," Deep-Sea Res. Pt. I-Oceanogr. Res. Papers **56**, 2175-2192 (2009).
19. G. E. Kim, A. Gnanadesikan, and M. A. Pradal, "Increased Surface Ocean Heating by Colored Detrital Matter (CDM) Linked to Greater Northern Hemisphere Ice Formation in the GFDL CM2Mc ESM," J. Clim. **29**, 9063-9076 (2016).

20. V. J. Hill, "Impacts of chromophoric dissolved organic material on surface ocean heating in the Chukchi Sea," J. Geophys. Res.-Oceans **113** (2008).
21. E. J. D'Sa, R. G. Steward, A. Vodacek, N. V. Blough, and D. Phinney, "Determining optical absorption of colored dissolved organic matter in seawater with a liquid capillary waveguide," Limnol. Oceanogr. **44**, 1142-1148 (1999).
22. R. Röttgers, and R. Doerffer, "Measurements of optical absorption by chromophoric dissolved organic matter using a point-source integrating-cavity absorption meter," Limnol. Oceanogr. -Methods **5**, 126-135 (2007).
23. P. Naik, and E. J. D'Sa, "Phytoplankton light absorption of cultures and natural samples: comparisons using two spectrophotometers," Opt. Express **20**, 4871-4886 (2012).
24. A. A. Andrew, R. Del Vecchio, A. Subramaniam, and N. V. Blough, "Chromophoric dissolved organic matter (CDOM) in the Equatorial Atlantic Ocean: Optical properties and their relation to CDOM structure and source," Mar. Chem. **148**, 33-43 (2013).
25. R. L. Miller, M. Belz, C. Del Castillo, and R. Trzaska, "Determining CDOM absorption spectra in diverse coastal environments using a multiple pathlength, liquid core waveguide system," Cont. Shelf Res. **22**, 1301-1310 (2002).
26. M. Belz, P. Dress, A. Sukhitskiy, and S. Liu, "Linearity and effective optical pathlength of liquid waveguide capillary cells," in SPIE Conference on Internal Standardization and Calibration Architectures for Chemical Sensors(SPIE, 1999), pp. 271-281.
27. M. I. Heller, K. Wuttig, and P. L. Croot, "Identifying the Sources and Sinks of CDOM/FDOM across the Mauritanian Shelf and Their Potential Role in the Decomposition of Superoxide (O2-)," Front. Mar. Sci. **3**, 132 (2016).
28. L. A. Zimmer, and G. A. Cutter, "High resolution determination of nanomolar concentrations of dissolved reactive phosphate in ocean surface waters using long path liquid waveguide capillary cells (LWCC) and spectrometric detection," Limnol. Oceanogr. -Methods **10**, 568-580 (2012).
29. M. Novak, A. Mannino, N. Nelson, E. D'Sa, R. Miller, J. Werdell, R. Del Vecchio, C. Del Castillo, J. Chaves, J. Francois-Berthon, E. Boss, M. Tzortziou, A. Neeley, S. Freeman, A. Bricaud, R. Röttgers, A. Matsuoka, M. Belz, and N. Blough, "Measurements of CDOM absorption spectra using different instruments and techniques: A round robin exercise and extensive field data set," presented at the Ocean Optics XXII Conference, Portland, ME, US (2014).
30. F. P. Chavez, K. R. Buck, R. R. Bidigare, D. M. Karl, D. Hebel, M. Latasa, L. Campbell, and J. Newton, "On the chlorophyll-a retention properties of glass-fiber GF/F filters," Limnol. Oceanogr. **40**, 428-433 (1995).
31. J. M. Sullivan, M. S. Twardowski, J. R. V. Zaneveld, C. M. Moore, A. H. Barnard, P. L. Donaghay, and B. Rhoades, "Hyperspectral temperature and salt dependencies of absorption by water and heavy water in the 400-750 nm spectral range," Appl. Opt. **45**, 5294-5309 (2006).
32. R. Röttgers, D. McKee, and C. Utschig, "Temperature and salinity correction coefficients for light absorption by water in the visible to infrared spectral region," Opt. Express **22**, 25093-25108 (2014).
33. M.I. Heller, D. M. Gaiero, and P. L. Croot, "Basin scale survey of marine humic fluorescence in the Atlantic: Relationship to iron solubility and H2O2," Global Biogeochem. Cycles **27**, 88-100 (2013).
34. Y. Q. Zong, S. W. Brown, B. C. Johnson, K. R. Lykke, and Y. Ohno, "Simple spectral stray light correction method for array spectroradiometers," Appl. Opt. **45**, 1111-1119 (2006).
35. S. Nevas, G. Wubbeler, A. Sperling, C. Elster, and A. Teuber, "Simultaneous correction of bandpass and stray-light effects in array spectroradiometer data," Metrologia **49**, S43-S47 (2012).
36. N. B. Nelson, D. A. Siegel, C. A. Carlson, C. Swan, W. M. Smethie, and S. Khatiwala, "Hydrography of chromophoric dissolved organic matter in the North Atlantic," Deep-Sea Res. Pt. I-Oceanogr. Res. Papers **54**, 710-731 (2007).